

STUDY OF MOLTEN ALUMINIUM CLEANING PROCESS USING PHYSICAL MODELLING AND CFD

Jin L Song¹, Fabio Chiti^{2,3}, Waldemar Bujalski², Alvin W Nienow² Mark R Jolly¹

¹Interdisciplinary Research Centre, School of Engineering, The University of Birmingham, Edgbaston,
Birmingham B15 2TT, U.K.

²Department of Chemical Engineering, School of Engineering, The University of Birmingham, Edgbaston,
Birmingham B15 2TT, U.K.

³Dipartimento di Ingegneria Chimica, Via Diotisalvi 2, Pisa 56126, Italy

Keywords: Molten Aluminum, CFD, Impeller, PIV, Mixing

Abstract

Furnace treatment is an important step during molten aluminium production by which the dissolved hydrogen and solid impurity particles are removed. Conventionally, a chlorine/inert gas mixture is used for this purpose injected into the molten metal via a simple lance. In order to meet new requirements for furnace emissions and improve efficiency, mechanical agitation through an impeller is becoming more widely used. In this research, the homogenization behaviour of both lance bubbling and mechanical agitation by impeller has been investigated experimentally and numerically. It can be concluded that under the same mean specific energy dissipation rates, the velocity magnitude for mechanical agitation process is about ten times bigger than that for the lance bubbling process, and the mixing time for the mechanical agitation process are much lower than that for the lance bubbling process, so better cleaning or fluxing would be expected.

Introduction

The mechanical properties of aluminium products very much depend upon the cleanliness of the molten aluminium. The cleanliness is normally measured by the hydrogen content, alkali elements and non-metallic inclusions. When present in a cast product, these gaseous and solid particles can cause a variety of property changes including edge cracking in aluminium sheet production [1], porosity formation during solidification [2], reduction in the fatigue strength and increase in corrosion rate [3]. Traditionally a chlorine/inert gas mixture was injected into the liquid aluminium through a static lance or steel wand sometimes containing a porous plug. In this process, the gas, in the form of discrete bubbles, rises to the top surface. Solid impurities may be lifted to the melt surface after being wetted or may react with the gas. Alkalies react with the gas to produce harmless salts which rise to the melt surface and hydrogen is removed by diffusion into the gas bubbles and burning off at when they reach the atmosphere. However this process generates large gas bubbles which are not well distributed in the melt. This results in ineffective mass transfer and reaction and therefore poor utilization of chlorine gas. To compensate for the inefficiency of furnace fluxing excess chlorine gas is used which leads to high production costs and gives rise to a potentially severe

environmental problems as it leaves the reactor. In order to improve the removal efficiency and use as little chlorine gas as possible in industrial holding furnaces rotary gas/salt fluxing technology (RGI/RFI rotary fluxing injection) has been introduced [4]. The industrial implementation of the rotary gas/salt fluxing technology has proven to give metallurgical and environmental benefits over the traditional chlorine fluxing process in terms of the emission requirements and removal efficiency of dissolved hydrogen, alkali metals and non-metallic inclusions found in molten aluminium [5]. In recent years predicting homogenization using CFD has been achieved [6,7,8]. In this research physical modelling and CFD simulation of the homogenization time has been measured using decolorization experiments and predicted using CFX5.6 for both single lance bubbling and the mechanical agitation process. The results illustrate clearly that RGI/RFI mechanical agitation fluxing is superior to the gas bubbling process.

Physical model set-up

The dimension of the industrial partners' melting furnaces vary in terms of the tonnage but they are all generally shallow and have a large surface area in order to maintain good heat transfer between the melt and the burners. In the current project a water tank (Figure 1) which was a scaled down representation of a typical industrial furnace was constructed. The laboratory 1 model was used for both lance bubbling and mechanical agitation system. The dimensions were: length 650 mm, width 254 mm and height 130 mm. Water was chosen as the fluid because its kinematic viscosity is similar to that of liquid aluminium [9]. Air was assumed to be the best way of modelling the chlorine gas (or the diluted mixture with nitrogen/argon) [10].

To simulate lance bubbling process the air was introduced through a single lance (a glass tube with a bore of 1mm) positioned on the centre line of the water tank ($y=0$) at a selected angle to the base with the end positioned about $z=10$ mm from the bottom and $x=200$ mm from one end of the longest dimension. For the mechanical agitation process, the impeller was positioned at a similar place as the lance, i.e. at a particular entry angle with the middle of the end the shaft positioned at $z=20$ mm and $x=200$ mm from one end of the tank. The impeller used Figure 2, is also a scaled down version of an industrial impeller and has five blades

and very high ratio between the blade thickness and impeller diameter. Decolourization experiments, in which $\text{Na}_2\text{S}_2\text{O}_3$ was added to the water using iodine as an indicator following procedures described by Cronin and Nienow [11], were carried out in order to compare the efficiency of gas bubbling and the mechanical agitation process. The mixing time was measured by recording the colour change.

In order to compare the effectiveness of mixing between the lance bubbling and the mechanical agitation process, the mean specific energy dissipation rate, $\bar{\varepsilon}_T$, parameter was chosen to link the two processes. In the case of gas bubbling, the full thermodynamic relationship for $\bar{\varepsilon}_T$ can be simplified for shallow liquids [12] to give formula (1):

$$\bar{\varepsilon}_T = g v_s \rho_L \quad (1)$$

For the case of the mechanical agitation, it is estimated by the formula (2):

$$\bar{\varepsilon}_T = \frac{P_0 \rho_L N^3 D^5}{V} \quad (2)$$

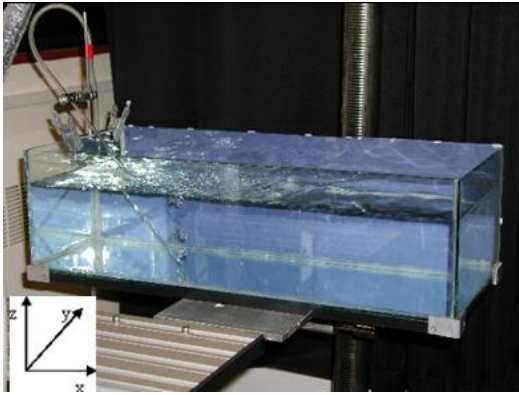


Figure 1: Water tank used for lance bubbling and mechanical agitation.

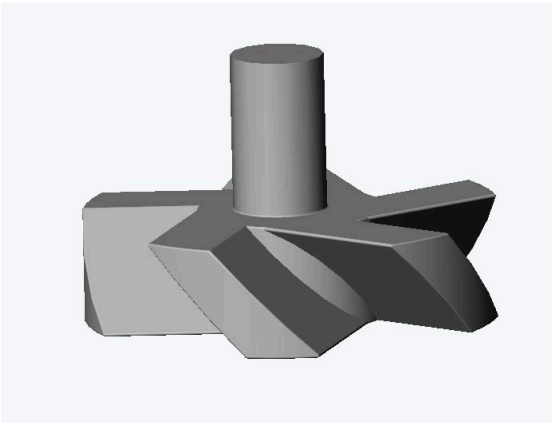


Figure 2: The scaled down impeller used for mechanical agitation.

Numerical Simulation

In the present research Flow-3D and CFX5.6 were used to simulate the process. Generally both codes used Navier-Stokes equations to describe fluid flow. The set of equations solved are continuity equation (3) and momentum equation (4):

$$\frac{\partial \rho}{\partial t} + \text{div}(\rho \mathbf{U}) = 0 \quad (3)$$

$$\frac{\partial \rho \mathbf{U}}{\partial t} + \text{div}(\rho \mathbf{U} \otimes \mathbf{U}) = \text{div}(-\mathbf{P}\delta + \mu(\nabla \mathbf{U} + (\nabla \mathbf{U})^T)) + \mathbf{S}_M \quad (4)$$

Where: ρ is the fluid density; \mathbf{U} is velocity vector; \mathbf{P} is the pressure; δ is identity matrix; \mathbf{S}_M is the momentum source.

In the case of lance bubbling the purge gas, in the form of bubbles, is considered as a dispersed phase and based on experimental observation an average bubble diameter 5 mm is assumed. The dispersed phase zero equation is used for its turbulence models. The water phase is the continuous phase. K- ε is chosen for its turbulence model. Density difference and particle model were chosen for buoyancy and interface transfer model. The surface tension between the two phases is 0.073 N/m. In the case of mechanical agitation, two domains are defined, one is the rotating domain of impeller, and the other domain is the stationary tank. Multiple frames of reference (MFR) technique was used to connect the two domains involved. Particle image velocimetry (PIV) was used to obtain instantaneous liquid velocities, in which the water is seeded with small ($\sim 10\mu\text{m}$) buoyant particles and illuminated with a plane sheet of laser light. As the particles have nearly the same density as water, they act as flow followers in the local transient velocity field without disturbing the flow itself. The transient flow pattern of the liquid within the light sheet is calculated from the displacement of the particles between successive images of the flow field [13].

In order to predict the mixing time (T_{90} or T_{95}), an additional variable, marker, for water is created, and the volumetric source is assigned for this additional variable. The marker concentration is calculated by solving the generalized scalar transport equation (5):

$$\frac{\partial \phi}{\partial t} + \text{div}(\mathbf{U}\phi) = \text{div}((\rho D_\phi + \frac{\mu_t}{S_{ct}})\text{div}(\frac{\phi}{\rho})) + S_\phi \quad (5)$$

Where ρ is the water density, \mathbf{U} is the water velocity, ϕ is the additional variable, S_ϕ is volumetric source, D_ϕ is the kinematic diffusivity for the additional variable, μ_t is the turbulence viscosity, S_{ct} is the turbulence Schmidt number. Firstly steady state simulations were carried out, then a transient simulation was run based on the steady state results in order to predict the mixing time. By comparing the value of this additional variable of individual points with the average additional variable value, the time for T_{90} and T_{95} can be decided. In the present research, typically five monitoring points are defined within the tank (figure 3) of which one is in the middle part of the tank, two are in the left side of the tank, and the other two are in the right side of the tank.

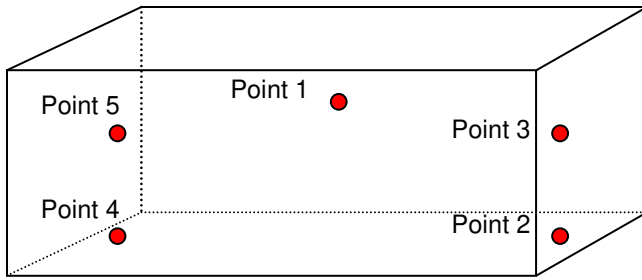


Figure 3 Showing the five monitor points within the tank

Results and Discussions

Similarly to the dimensions of the water tank, the volumetric flow rate is also scaled down based on the industrial operation data. In the present research, the volumetric flow rate of single lance bubbling process was chosen 1.0 l/min. Based on formula (1) and (2), for the same mean specific energy dissipation rates, the equivalent impeller rotation speeds is 303 rpm. Figure 4 shows the concentration profiles of the additional variable, marker, for the five monitoring points (indicated in figure 3), and the average value (466 kg/m³) for the lance bubbling process. From the figure, it can be found that before 25 seconds or so, the additional variable values for the monitor points at both ends are zero, this means the mixing did not reach both ends of the tank. After 25 seconds, the additional variable values of the monitor points 2 – 5 gradually increase with time. It can be found that at the beginning of the process, the value of monitor point 1 quickly reaches a very high value, then gradually converges to an average of 466 kg/m³, while the values of monitoring points 2 and 4 go above the average value, and those of the monitor points 3 and 5 are always lower than the average value. As the time increases the values of these monitor points all converge to the average value. Since the source of the additional variable is just under the top surface at the lance tip position, the monitor point 1 is the nearest to it. So the additional variable value at this point will quickly increase to a high value at the beginning of the process. While for the monitor points 3 and 5, they are a long way from the additional variable source, and there are flow circulations (which are shown in figure 5) over there. So the additional variable values will slowly increase to the average value.

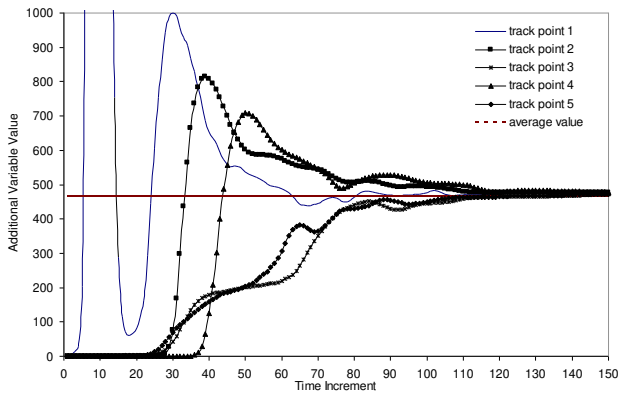


Figure 4 Additional variable values of monitoring points, average, and T90 in the case of lance bubbling process.

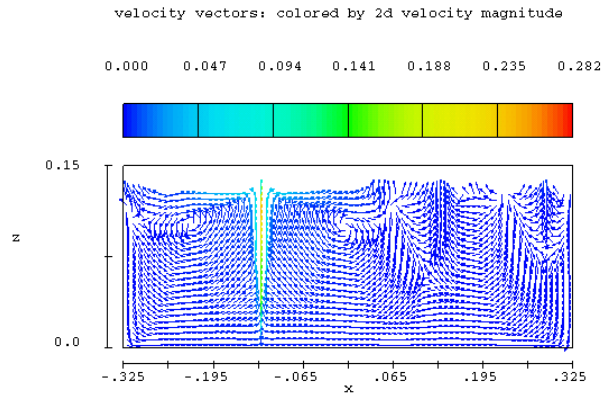


Figure 5 Velocity vector in XZ plane showing three circulations in the flow field

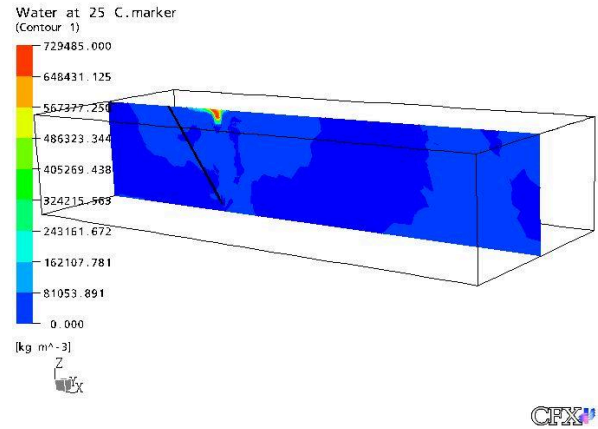


Figure 6 Contour plot showing additional variable, marker, value at simulation time 1 second.

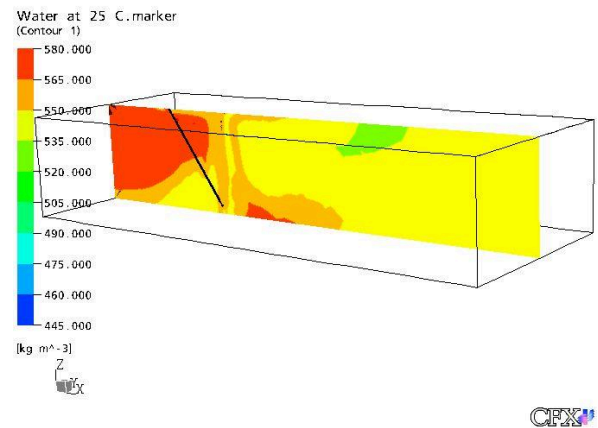


Figure 7 Contour plot showing additional variable, marker, value at simulation time 135 second.

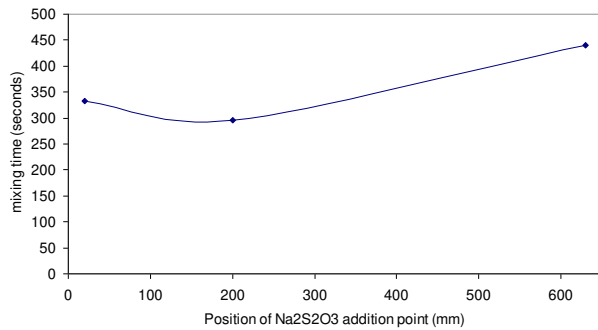


Figure 8 Mixing time for lance bubbling as a function of addition position of the tracer at volumetric flow rate 1.0 l/min.

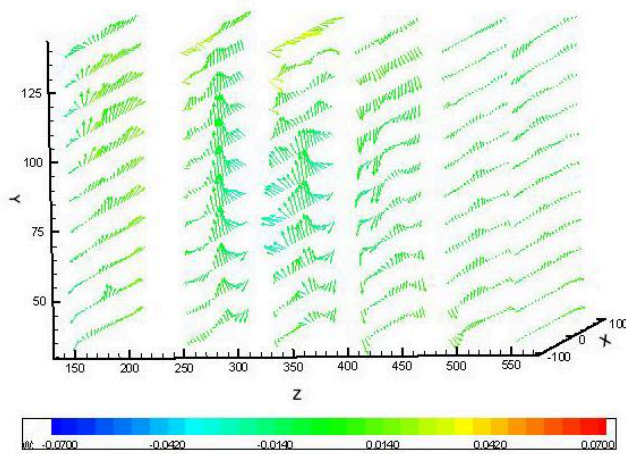


Figure 9 Vector plot showing velocity magnitudes at six cross sections for lance bubbling process at volumetric flow rate 1.0 l/min.

The total additional variable added at the source point is 10.0 kg, so it can be calculated that the T90 and T95 are 420 and 443 kg/m³. According to the additional values in figure 4, it can be calculated that the T90 and T95 are about 95 and 135 seconds. Figure 6, 7 show the contour plots of the additional variable, marker, values at the computational time 1 and 135 seconds. At the beginning of the computation, the additional variable value should be quite high at the source point, which is clearly shown in figure 6. At 135 seconds most of the additional variable values are over 443 kg/m³ (figure 7). The mixing time measured from decolourization experiments is 295 seconds. Two factors contributed to the difference between the predicted and measured mixing time. Firstly in the CFD model diffusivity is not taken consideration and it is assumed that instantaneous mixing purely depending on the flow field occurs. However in the decolourization experiments the mixing time is also dependent on the diffusion process. This can be verified in figure 8 which shows the effect of changing the position of the addition point and show different mixing times. Secondly only five monitor points were defined in the present research, which is unlikely to demonstrate the whole tank behaviour. So more CFD works need to be done to investigate the effects of diffusivity and the number of monitor

points on the mixing time. Figure 9 shows the six cross sections (150 mm, 250 mm, 330 mm, 410 mm, 490 mm, and 555 mm) velocity vectors measured using PIV, and figure 10 shows the three cross sections (330 mm, 410 mm, 555 mm) velocity contour plots. It can be found that PIV measured data is in reasonable agreement with CFD prediction.

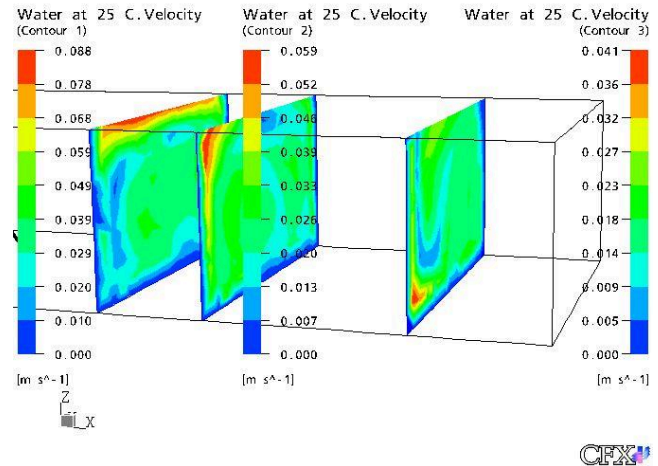


Figure 10: Velocity contour plot from CFD of three cross sections for lance bubbling process at volumetric flow rate 1.0 l/min.

For the mechanical agitation process, the impeller shaft is inclined at 45° relative to the liquid surface. Figure 11 shows the absolute pressure distribution around the impeller blade. It can be found that a high pressure is build up under the blade, and low pressure above the blade. This is consistent if the impeller rotates clockwise. Figure 12 shows the velocity vector plot measured from PIV technique at the five selected cross sections (250 mm, 330 mm, 410 mm, 490 mm, 555 mm). Figure 13 shows CFD predicted velocity contour plot at the three cross sections (330 mm, 410 mm, 555 mm). It can be found that the CFD predicted velocity magnitude is higher than that measured from PIV technique. The reason for this is PIV cannot measure the velocity over the 20 mm range near the bottom of the tank. However for the mechanical agitation process, the highest velocity appears to be near the bottom of the tank. In order to compare the mixing efficiency between the lance bubbling and the mechanical agitation process the same decolourization experiment was also carried out as that in the lance bubbling process and the mixing time is 83.7 seconds which is much faster than that (295 seconds) in the lance bubbling process. This can be explained from the velocity field from figures 11 and figure 13. Even though the two processes had the same mean specific energy dissipation rates, the velocities for the mechanical agitation process are about twice times bigger than those in the lance bubbling process. CFD simulation was also carried out using liquid aluminium for the mechanical agitation process, and figure 14 shows the predicted velocity contour plot at the three cross sections (330 mm, 410 mm, 555 mm). Comparing the results with those in figure 13 for water it can be seen that the absolute velocities overall are lower for the aluminium because of the higher density relative to water but the flow patterns are more or less the same.

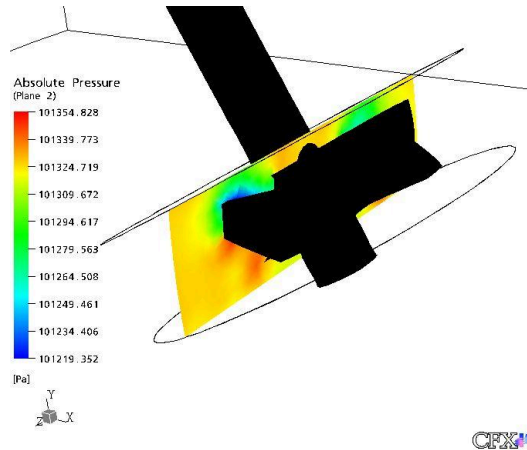


Figure 11: Pressure distribution on both sides of the blades with impeller rotation 303 rpm.

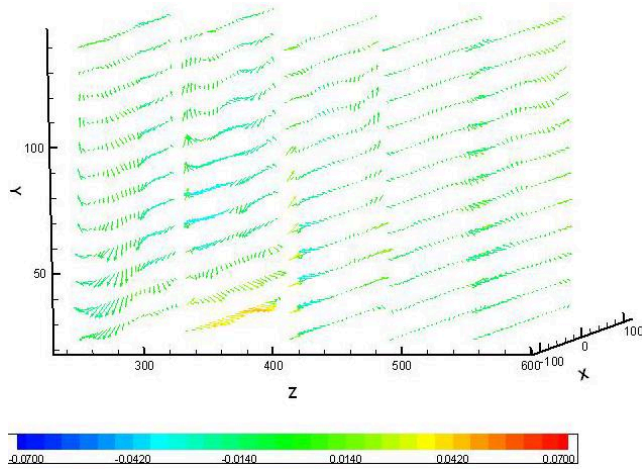


Figure 12 Vector plot showing velocity magnitudes at five cross sections for mechanical agitation at rotating speed 303 rpm.

Conclusions

In the present work a laboratory water tank was set up based on real industrial molten aluminium furnace dimensions. Both gas bubbling and mechanical agitation process were simulated by cold modelling and CFD analysis. The velocity fields measured by PIV system were compared with CFD prediction it was found that at the same mean specific energy dissipation rate and the same cross section, the velocity magnitude for mechanical agitation process is about ten times bigger than that for the lance bubbling process. Experimental decolorisation tests also showed that the mixing time of the mechanical agitation through impeller is much faster than that for the lance bubbling process. CFD modelling of water and aluminium were compared and although the velocities predicted in aluminium were lower the velocity profiles were similar. It can be concluded that the mechanical agitation through

impeller should give a better fluxing result than the conditional lance bubbling process under the same mean specific energy dissipation rate.

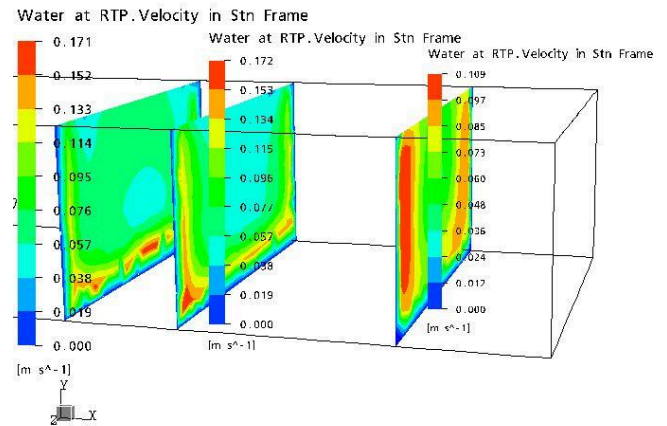


Figure 13: Velocity contour plot from CFD of three cross sections for mechanical agitation at the rotating speed of 303 rpm (water).

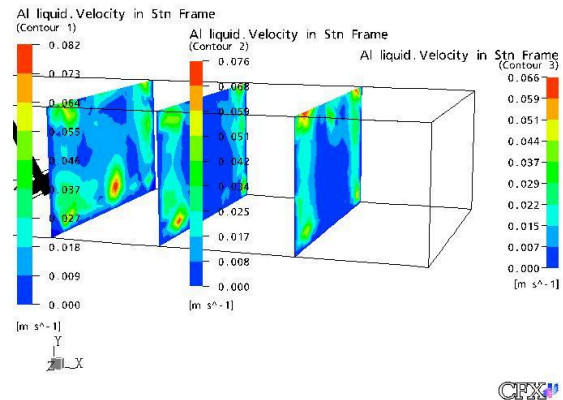


Figure 14: Velocity contour plot from CFD of three cross sections for mechanical agitation at the rotating speed of 303 rpm (liquid aluminium).

Acknowledgements

The authors, JLS and WB, would like to acknowledge the financial support from EPSRC for the project "Physical and computational modeling of non-chlorine cleaning of aluminium in furnace as a tool for cleaning process design". Thanks are also given to our industrial partners, N-Tec, MQP/STAS, VAW, Norton Aluminium, Carney Ltd, and Alba, for both financial and technical support to this project

References

1. C.J. Simensen, M. Nilmani, (1996), "A computer model for alkali removal from molten aluminium", *Light Metals 1996*, TMS (The Minerals, Metals & Materials Society, 995 - 1000.
2. J.G. Steven,, H. Yu, (1986), "Mechanism of sodium, calcium and hydrogen removal from an aluminium melt in a stirred tank reactor – the ALCOA 622 process", *Light Metals 1988*, TMS(The Minerals, Metals & Materials Society, 437 - 443.
3. T.A. Engh, (1992), "Principle of Metal Refining", *Oxford University Press, New York, NY*, pp. 1-35
4. J.F. Bilodean, C. Lakroni, Y. Kocaefe, (2001), "Modelling of rotary injection process for molten aluminium processing", *Light Metals 2001*, TMS(The Minerals, Metals & Materials Society, 1009-1015.
5. P.J. Flisakowski, J.M. McCollum, R.A. Frank, (2001), "Improvements in Cast Shop Processing Using Pyrotek's HD-2000 and PHD-50 Rotary Injector System", *Light Metals 2001*, TMS(The Minerals, Metals & Materials Society, 1041-1047.
6. W. Bujalski, Z. Jaworski, N. Otomo and A.W. Nienow, (1998), An experimental and CFD study of homogenisation with dual Rushton turbines. *Proc 1998 IChemE Research Event*, University of Newcastle Upon Tyne, 7-8 April 1998, Newcastle, U.K.
7. Z. Jaworski, W. Bujalski, N. Otomo, A.W. Nienow, CFD study of homogenization with dual Rushton turbines – comparison with experimental results, *Trans IChemE*, vol 78, part A, April 2000, 327-333
8. A.W. Patwardhan, CFD modelling of jet mixed tanks, *Chemical Engineering Science* 57 (2002) 1307-1318
9. J.J.J. Chen, J.C. Zhao, P. Lacey & T. Gray, (2001), "Flow pattern detection in a melt treatment water model based on shaft power measurements", *Light Metals 2001*, TMS(The Minerals, Metals & Materials Society, 1021-1025.
10. K.A. Carpenter and M.J. Hanagan, (2001), "Efficiency modelling of rotary degasser head configurations and gas introduction methods, part1-water tank tests", *Light Metals 2001*, TMS(The Minerals, Metals & Materials Society, 1017-1020.
11. Cronin, D.G., Nienow, A.W and Moody, G.W. (1994), "*Food Bio-products Processing, Trans IChemE (Part C)*, 72, 35 - 40".
12. C.D. Boswell, J. Varley, L. Boon, C.J. Hewitt, A.W. Nienow, (2003), Studies on the impact of mixing in brewing fermentation – Comparison of methods of effecting enhanced liquid circulation, *Food and Bio-products Processing*, 81, 33 – 39.
13. C. Gray and C.A. Greated, (1987), "The application of particles image velocimetry to study of water wave", *Optics and laser in engineering*, 9, 265 – 276

Study of molten aluminium cleaning process using physical modelling and CFD

Song, Jin L.

2004-03-18

Song JL, Chiti F, Bujalski W, et al., (2004) Study of molten aluminium cleaning process using physical modelling and CFD. In: Light Metals 2004: 133rd TMS Annual Meeting, 14-18 March 2004, Charlotte, NC, USA. pp. 743-748

<https://dspace.lib.cranfield.ac.uk/handle/1826/20450>

Downloaded from CERES Research Repository, Cranfield University